49

When Light Microscope Resolution Is Not Enough: Correlational Light Microscopy and Electron Microscopy

Paul Sims, Ralph Albrecht, James B. Pawley, Victoria Centonze, Thomas Deerinck, and Jeff Hardin

INTRODUCTION

Early Correlative Microscopy

Notwithstanding the many ways, amply documented elsewhere in this book, in which fluorescent light microscopy can elucidate biological structure and function, there are times when the available spatial resolution is just not sufficient to answer the biological question. Consequently, there is a need to follow up the initial light microscope (LM) findings by subsequently viewing the LM specimens in the transmission or scanning electron microscope (TEM or SEM). Correlative microscopy of this type has a long history. In 1973, shortly after LM stains had been developed that identified T- and B-lymphocytes, Wetzel viewed the same exact cells, first in the LM and then in the SEM to show that being a T or a B cell bears no relation to whether the cells appeared to be "rough" or "smooth" when viewed in the SEM (Wetzel *et al*., 1973).

Somewhat later, Sepsenwol used time-lapse studies in the LM followed by high-voltage electron microscopy (HVEM) and SEM to study the unusual protein on which *Ascaris* sperm motility is based (Pawley *et al*., 1986; Sepsenwol *et al*., 1989; Sepsenwol and Taft, 1990).

Early 4D Microscopy

Albrecht and his group tracked the motion of colloidal gold–labeled proteins on the surface of activated platelets, using time-lapse, rectified, differential interference contrast (DIC), LM (Fig. 49.1), before determining the final position of the gold particles using both low-voltage SEM (LVSEM; Figs. 49.2, 49.3, and 49.4; Pawley, 1990, 1992) and HVEM (Figs. 49.5 and 49.6; Albrecht *et al*., 1989, 1992; Loftus *et al*., 1984).

This pioneering work did much to elucidate the mechanism of clot formation. It was possible in part because the platelet is small enough to be viewed in the HVEM as a critical-point-dried (CPD) whole mount and in part because the colloidal gold used to label the surface receptors of interest could be seen in the LM, the SEM and the HVEM. The LM allowed one to watch the movement of the Au-labeled, fibrinogen receptors; the LVSEM at 1 and 5 kV allowed one to see how these markers were bound to the surface (Pawley and Albrecht, 1988); and stereo views from the HVEM allowed one to correlate these surface changes with changes in the location and orientation of the cytoskeleton. The details of these early studies are found in the captions of Figures 49.1 through 49.9.

More recently, this group extended the technique by adding an additional, sensitive charge-coupled device (CCD) camera and an ingenious system of dichroic filters to permit them to image living cells using ultraviolet (UV) fluorescence at the same time that they were being viewed using rectified DIC. This has allowed them to follow the motion of the 20 nm gold particles in the DIC image while monitoring the intracellular Ca^{++} concentration using fura-2. As shown in the previous images, the binding of fibrinogen to the receptor (and associated receptor cross-linking) triggers a centripetal movement (edge to center) of the receptor–ligand complexes over the platelet surface. The new instrumentation has allowed them to determine that the movement of the receptors across the platelet surface coincides with a Ca^{++} transient (Fig. 49.10) and to do this on a platelet that they can view subsequently by LVSEM.

CORRELATIVE LIGHT MICROSCOPE/ELECTRON MICROSCOPE TODAY

Light Microscope and Electron Microscope Have Different Requirements

Because the structural details of electron microscope (EM) samples must be preserved in much greater detail and because almost all EM specimens must be viewed *in vacuo*, procedures for preparing them differ markedly from those used in the LM. Correlative studies can be segregated in several ways. The first way is based on the order in which observations are made:

1. The LM observations are made first, on fixed or living cells, and these are then prepared for EM.[1]
2. The preparation is fixed and stained before LM observation.
3. Cells incorporating fluorescent markers are prepared for thin-section TEM, but these are viewed in the LM just before being viewed in the EM.

[1] Because the act of observing a biological specimen in an EM subjects it to a flux of radiation so high that virtually all the organic molecules present (such as dyes or stains) are irretrievably damaged, there is seldom much point in viewing a specimen in an LM after it has been viewed in an EM. The exception to this rule is the quantum dot, a fluorescent label that, as discussed below, is not destroyed by being observed in the TEM.

Paul Sims, Ralph Albrecht, James B. Pawley, and Jeff Hardin • University of Wisconsin, Madison, Wisconsin 53706
Victoria Centonze • University of Texas Health Science Center, San Antonio, Texas 78229
Thomas Deerinck • University of California, La Jolla, California 92093

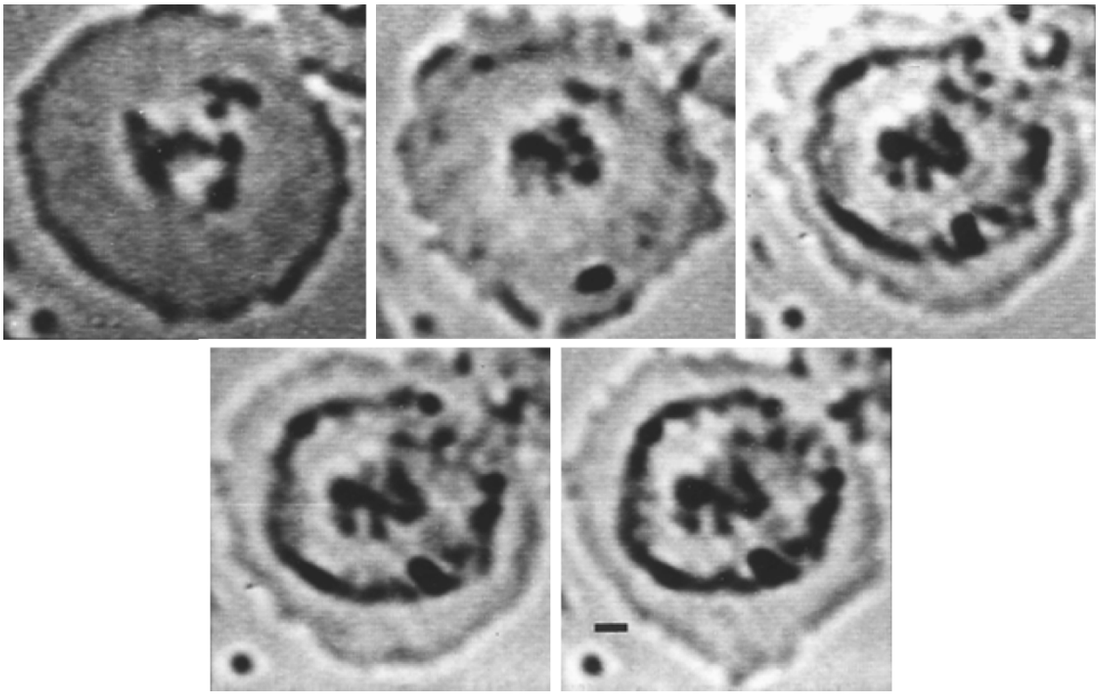

FIGURE 49.1. Time-series of DIC images showing initial binding of Au-conjugated fibrinogen (black) to the platelet surface membrane over the subjacent peripheral web and outer-filamentous zone of the cytoskeleton of a fully spread, substrate-adherent platelet. This label binds to the integrin receptor for fibrinogen on platelets. Over several minutes, bound labels are transported over the surface, towards the platelet center coming to rest, still on the membrane surface, but now overlying the inner filamentous zone. The platelet is then fixed, stained with osmium and uranyl-actetate, and dried by the critical-point procedure for subsequent LVSEM and HVEM. Bar = 1 μm.

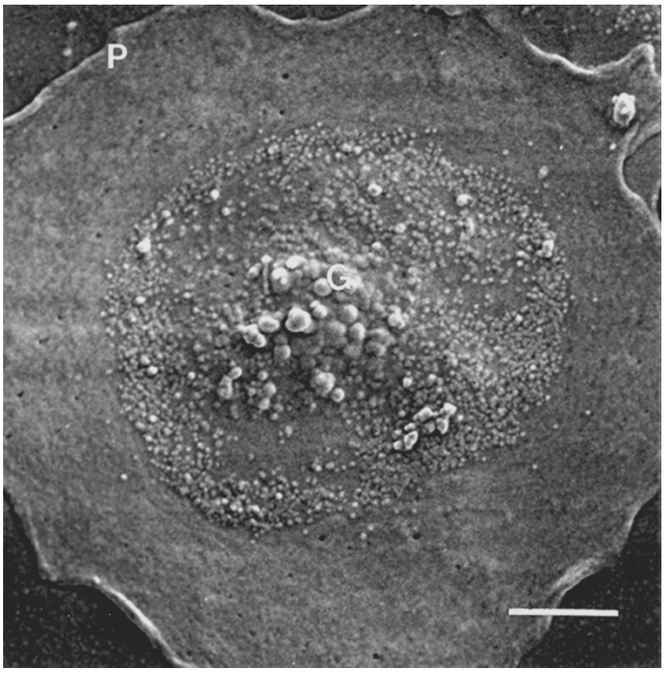

FIGURE 49.2. Surface image of the same uncoated platelet as Figure 49.1 viewed in LM at 1 kV accelerating voltage in a modified Hitachi S-900 SEM. It shows the platelet surface and labels in detail. What is actually seen is the platelet surface and the fibrinogen-covered individual gold particles. Bar = 1 μm.

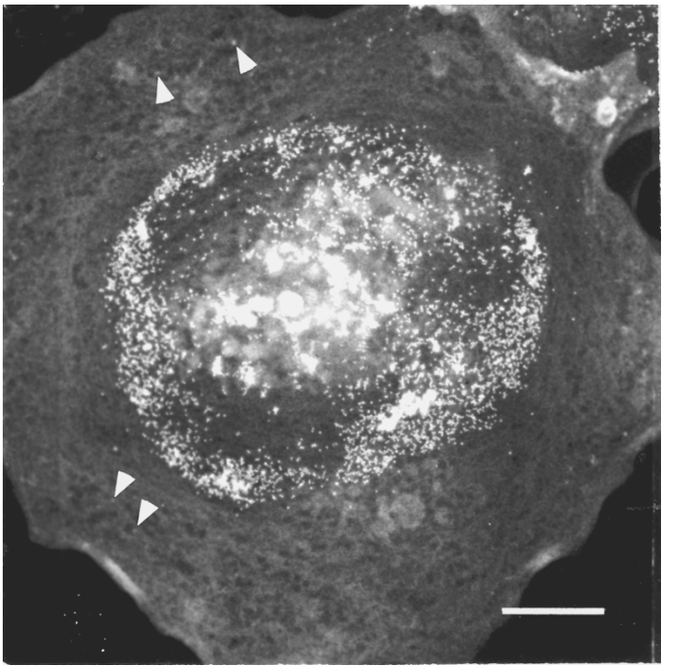

FIGURE 49.3. SEM at 5 kV, still in the SE mode. The increased beam penetration clearly demonstrates the location of the gold particles, bright spots, relative to stained internal cytoskeletal structures. However, surface structure is less apparent. Bar = 1 μm.

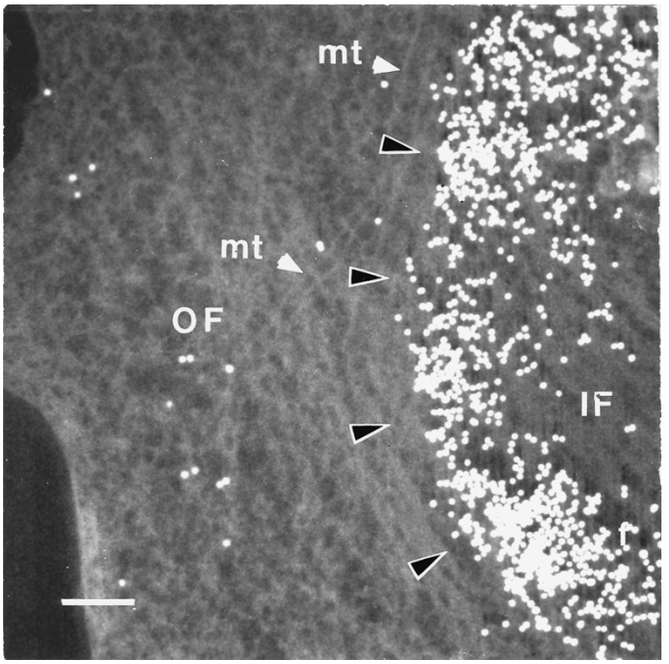

FIGURE 49.4. SEM at 20 kV and somewhat higher magnification. This demonstrates the relationship of the labels on the membrane surface to the underlying cytoskeletal organization. Bar = 0.25 µm.

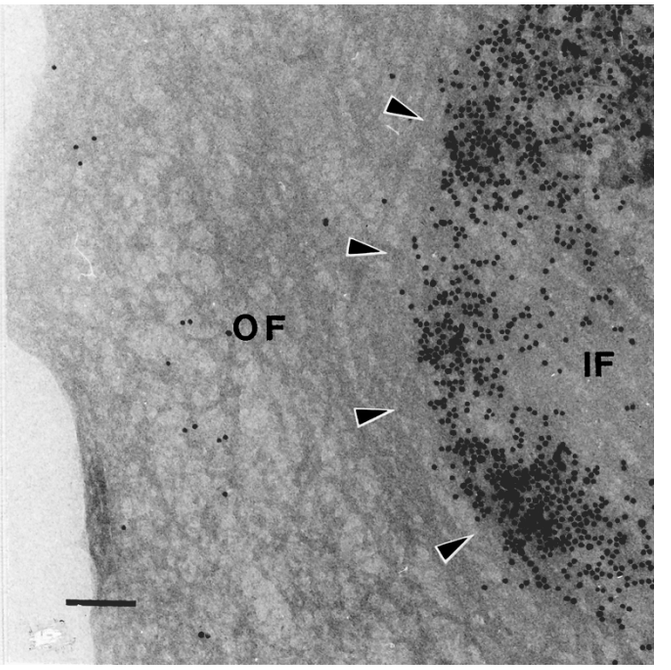

FIGURE 49.6. A higher magnification HVEM of the same area of the platelet as seen in Figure 49.4. P, peripheral web; OF, outer filamentous zone; IF, inner filamentous zone; G, granulomere; mt, microtubules; dark arrowheads, margin of inner filamentous zone; white arrowheads in Figure 49.3 point to labels trapped under the platelet. Bar = 0.25 µm.

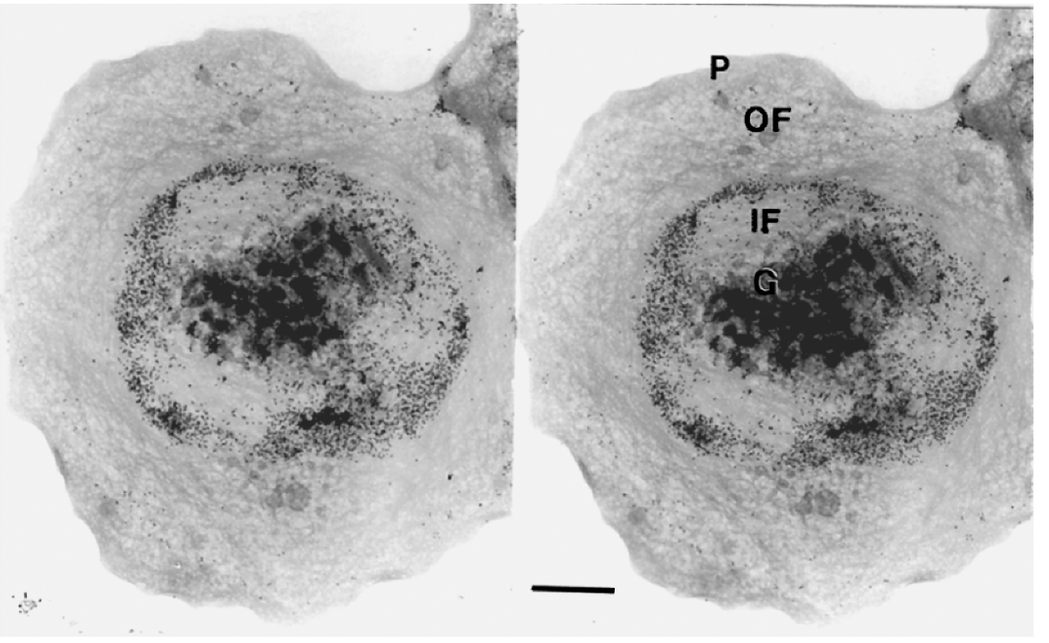

FIGURE 49.5. HVEM stereo-pair whole mount of the same platelet, which offers a clear view of the platelet cytoskeleton. The gold labels, black spots, are clearly seen in relationship to the subjacent platelet cytoskeleton. Bar = 1 µm.

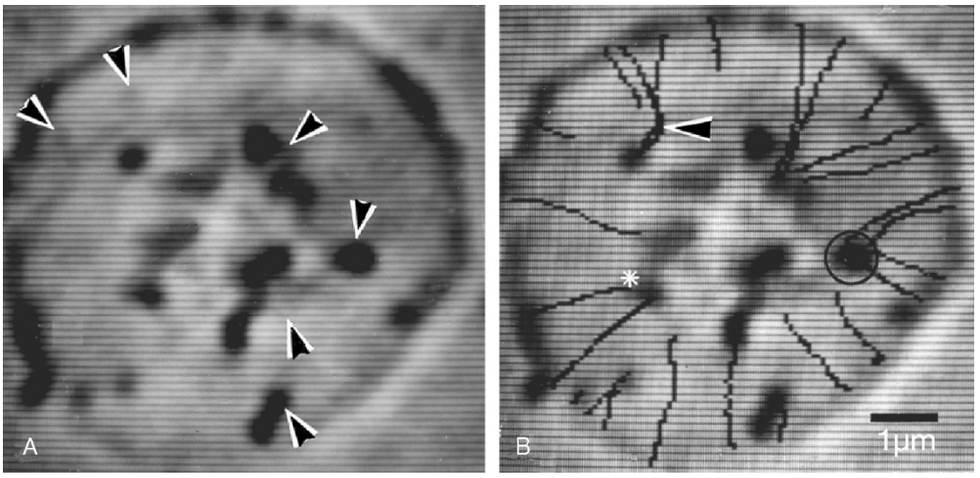

FIGURE 49.7. DIC imaging tracking of movement of individual label particles across the surface of a fully spread platelet.

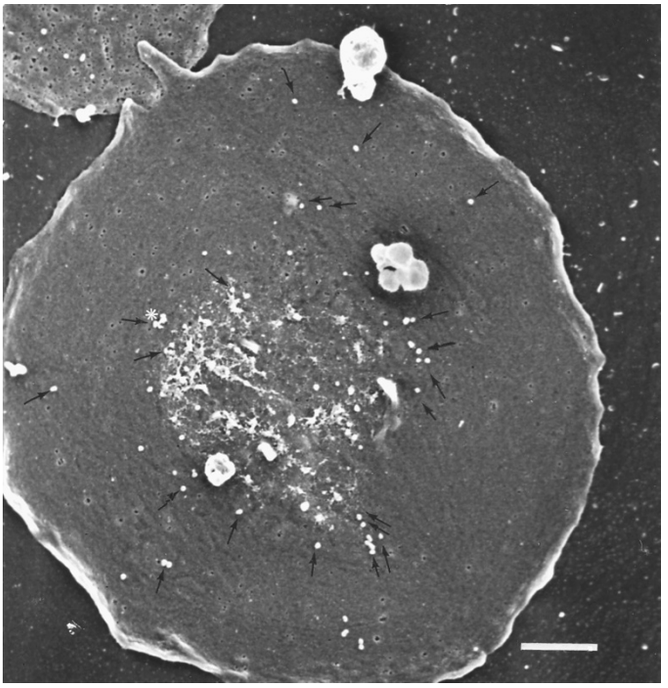

FIGURE 49.8. The same platelet, following fixation, staining, and dehydration, is seen via LVSEM at 1.5 kV accelerating voltage. The position of the individual tracked particles at the time of fixation relative to the platelet surface can be seen.

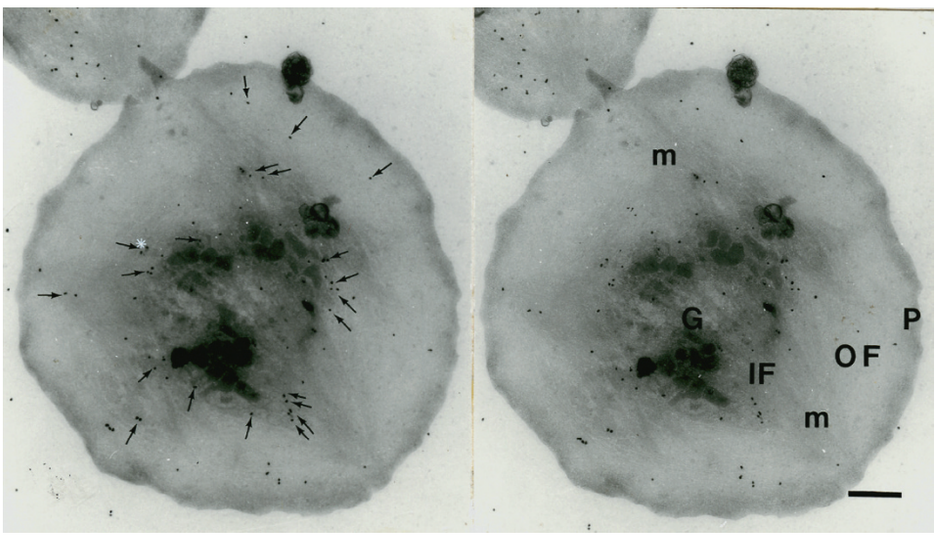

FIGURE 49.9. The same platelet, HVEM stereo-pair, demonstrating the position of the particle labels relative to internal structure. P, peripheral web; OF, outer filamentous zone; IF, inner filamentous zone; G, granulomere zone; m, microfilament bundles. Arrows point to individual labels also seen in Figure 49.8, asterisk indicates particle tracked in Figure 49.7 and seen in Figures 49.8 and 49.9. Labels fixed in transit generally still appear over the outer filamentous zone while labels that have completed their movement are generally seen over the inner filamentous zone. Bar = 1.0 μm.

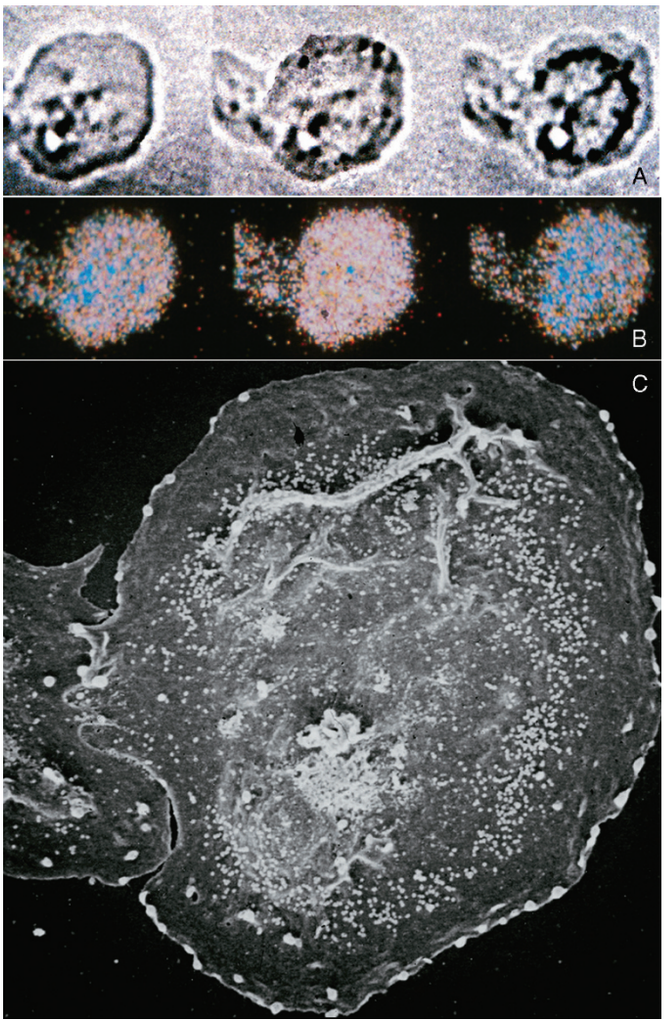

FIGURE 49.10. (A) and (B) show a platelet imaged simultaneously via DIC and UV fluorescence. In (A), the diffraction images of colloidal gold–fibrinogen particles can be followed over time as they move across the platelet surface. (B) Fura-2 340 nm/380 nm ratio images that provide a measure of the free internal [Ca^{++}] as the process proceeds (blue represents resting [Ca^{++}] levels while red and white show increasing [Ca^{++}]). Although the initial fibrinogen-binding produces no increase in free [Ca^{++}] (left panels), once the movement of the fibrinogen-receptor complexes is initiated, [Ca^{++}] is seen to increase (middle panels) until the movement is complete (right panels). (C) An LVSEM image of the same platelet shows the final position of the gold-fibrinogen-receptor complexes (bright spots) relative to platelet surface structure.

Another way of dividing correlative methods is between those using the TEM and those using the SEM. A final criterion that might be used to characterize correlative LM/EM studies is whether it is essential to view exactly the same cell using all methods or if it is sufficient to use the EM image merely to find out the general type of structures being labeled in the LM preparation. The following sections will include a brief review of recent studies illustrating all of these approaches.

Finding the Same Cell Structure in Two Different Types of Microscope: Light Microscope/Scanning Electron Microscope

Because both the LM and the SEM permit one to view quite large specimens, it is often easier to find the exact cell previously viewed in an LM using an SEM rather than a TEM. Centonze and coworkers used this combination to investigate the effect of fluorescence recovery after photobleaching (FRAP) on the molecular structure of the labeled structures. In FRAP, a structure or volume that has been labeled with fluorescent dye in a living cell is intentionally bleached and one then measures the rate at which fluorescence returns to the bleached area (see Chapters 5, 8, 9, 17, and 45, *this volume*). Alternatively, one may wish to derive inferences from the motion of the bleached area. One well-studied example is the motion of a band bleached across a mitotic apparatus made of fluorescent tubulin. In this case, the band did not move even though mitosis proceeded (Gorbsky *et al*., 1987). Centonze used the SEM to investigate this further.

To do this, gold was evaporated through an EM finder grid onto the surface of a glass coverslip to create a fiduciary pattern that could be seen in both the LM and the SEM. These coverslips were then mounted into a hole in the bottom of a plastic Petri dish using silicone grease and isolated, fluorescent microtubules were allowed to adhere to the glass. After obtaining reference transmission and fluorescence LM images, some of the microtubules not located over the gold were bleached, using 546 nm light from an argon-ion laser, for a measured period of time at a known power level. The preparation was then fixed, critical-point dried, coated with ion-beam-sputtered Pt, and viewed in a high-resolution, low-voltage SEM at 1.5 kV. Figure 49.11 shows the results. While a 10 ms pulse caused little visible damage, 30 ms caused total destruction. Fortunately, as is shown in Figure 49.12(A), it is possible to produce significant bleaching using a pulse only 1 ms in duration, a period thought unlikely to cause severe structural damage. It should also be noted that dissolution or disruption of microtubules could also be induced by repeated illumination under conditions used for normal fluorescence observations.

Figure 49.13 shows this system applied to bleaching microtubules in a living cell grown on a marked coverslip. In this case,

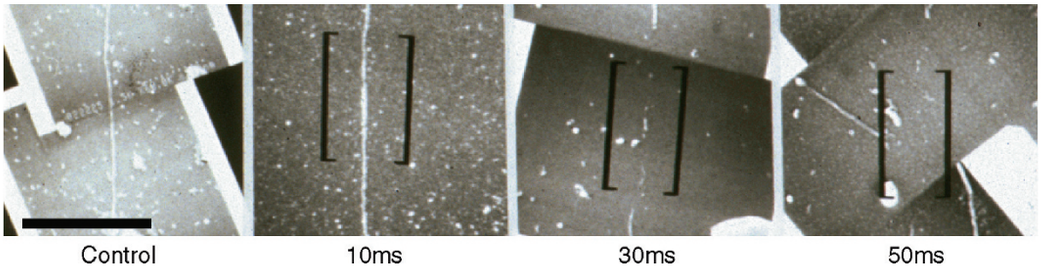

FIGURE 49.11. Low-voltage scanning electron micrographs of single fluorescent microtubules that had earlier been subjected to irradiation by a 546 nm bleaching beam for the times listed. Any exposure above 10 ms destroyed the microtubule.

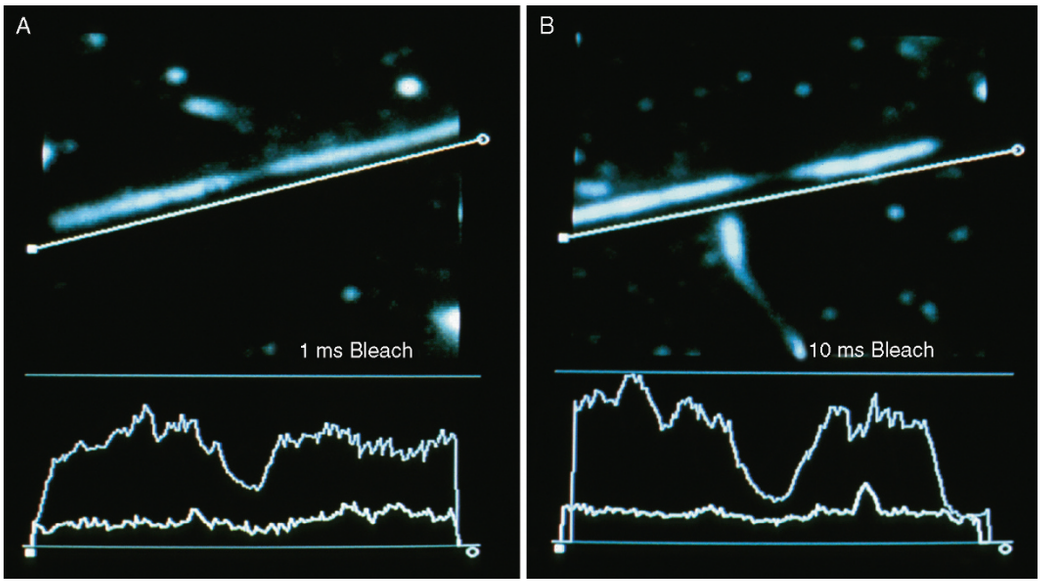

FIGURE 49.12. Fluorescence micrographs showing single microtubules, composed of *in vitro* polymerized microtubules made from rhodamine-conjugated tubulin, across which a bar has been bleached by exposure to a 546 nm laser beam for the noted times. (A) shows that substantial bleaching is produced by a 1 ms exposure, a level 10× lower (B) than that shown to produce structural damage in Figure 49.11. The plots below each image show the intensity along a line down the center of the microtubule (upper trace) and along the straight white line, showing the background signal (lower trace).

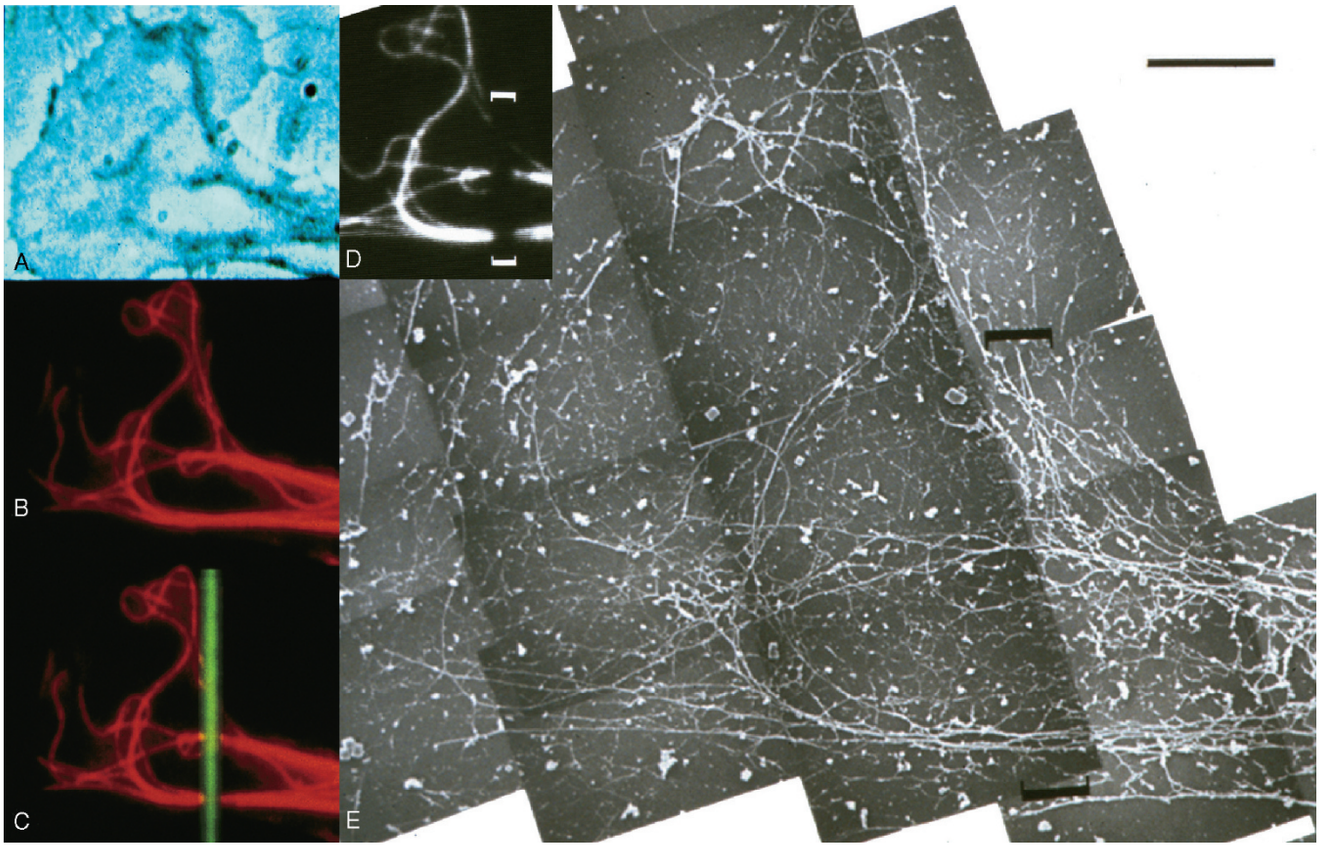

FIGURE 49.13. (A) Phase-contrast image of a spread cell containing microtubles made out of rhodamine-conjugate tubulin. (B) Fluorescence image of the same field. (C) Bleached bar and (D) fluorescence image of the same areas of the specimen after it has been prepared for SEM. (E) Tiled montage of low-voltage SEM images in which one can see that all the microtubules visible in the LM images, even those in the bleached zone (brackets), remain physically intact after the bleaching event.

fibroblast cells were grown on gold-sputtered, locator coverslips and injected with fluorescent derivatized tubulin. After the injected tubulin was allowed to incorporate into the microtubule cytoskeleton for at least 1 h, the injected cells were relocated using phase-contrast microscopy. Fluorescent microtubules were imaged both before and after photobleaching a discrete region [Fig. 49.13(D)]. Because the fixation protocol involved lysing the cells in Triton X-100 detergent before fixation in 2% glutaraldehyde in a cyto skeletal-stabilizing buffer containing, Pipes, Hepes, EGTA and Mg^{++} (PHEM) buffer, the montage of SEM images shows the cytoskeleton, rather than the cell membrane. In this case, bleach levels were low enough to create a photobleach mark without disrupting the microtubules so that all of the microtubules visible in the fluorescence image are visible in the SEM montage. LVSEM images of specimens bleached with higher power, or for a longer time, showed that the affected microtubules could be completely ablated. The ablation was documented in three ways: (1) the fluorescence recovery rates were observed to be different in the bleached region; (2) treatment with fluorescent anti-tubulin produced no staining in the photobleached region because the structures were destroyed; and (3) SEM images clearly show no microtubule structures in the photobleached region (data not shown). This correlational study should give pause to anyone convinced that the ONLY possible effect of photobleaching is that the dye in the irradiated volume becomes non-fluorescent. More insight into photodamage mechanisms is provided in Chapters 38 and 39.

Finding the Same Cell Structure in Two Different Types of Microscope: Light Microscope/Transmission Electron Microscope

Although correlative microscopy uses both light and electron microscopy to examine the same sample, each microscopic method produces contrast in a very different way. When viewing living biological specimens in the LM, one commonly uses phase, DIC, or more recently, fluorescence imaging. However, in the TEM, none of these factors produces significant contrast, and, in addition, the TEM specimen must be considerably thinner than most cells. To produce enough mass-thickness contrast to make biological structures visible in the TEM, one must somehow decorate them with heavy metal stains, such as uranyl–acetate and lead compounds. As a result, LM/TEM correlative methods generally depend on the use of some technique that will deposit heavy metals at or near the site of the fluorescent dye. Possibilities include double labeling with both fluorescent and Au-conjugated antibodies and using light captured by the fluorescent dye to initiate a chemical reaction that later results in the deposition of a heavy metal. Finally, quantum dots are particularly useful because they are both fluorescent and directly visible in the TEM (Niesman *et al*., 2004).

Correlative LM/TEM techniques are also complicated by the fact that the visible area of a TEM grid is usually less than 2 mm in diameter and quite a lot of this area is obscured by grid bars. Moreover, it is in general hard to keep track of changes in the orientation of specific structures in the LM specimen as the sample passes the many steps needed to prepare it for thin-section TEM. This can make it very difficult to find exactly the same feature using both methods, especially if the handedness of the image has been changed by the section having been mounted upside-down.

Making LM Labels Visible in the Transmission Electron Microscope

There are a few techniques that allow the same stained sample to be used for both light and electron microscopy. One of the most successful methods for doing this, called fluorescence photo-oxidation, was developed by Maranto (1982) and later extended to immunolabeling and *in situ* hydridization by Ellisman (Deerinck *et al*., 1994). It relies on the fact that, when certain fluorescent dyes, such as eosin, are excited in the presence of diaminobenzidine (DAB), the reactive oxygen produced by the triplet-excited fluorescent compound causes the DAB to form a deposit very close to the reaction site. This deposit can then be stained with considerable specificity with osmium tetroxide (Fig. 49.14), rendering it visible by both transmitted light and electron microscopy. Because the reaction is limited to only the region near the excited fluorescent dye, the precise area can be located in the epoxy-embedded specimen by light microscopy and then prepared for thin section electron microscopy.

More recently, this group has adapted the tetracysteine genetic marking technique to produce the reactive oxygen needed to deposit the DAB in labeled cells (Griffin *et al*., 1998; see Chapter 16, *this volume*). In this technique, a tetracysteine tag sequence is

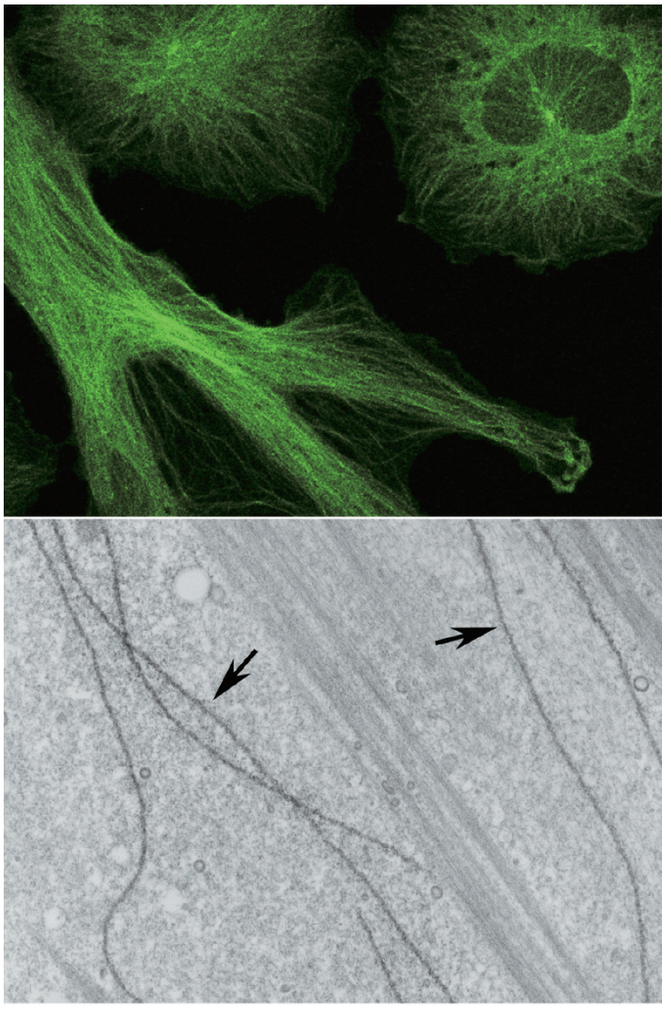

FIGURE 49.14. (A) Using immunofluorescently stained bovine aortic epithelial cells for both light and electron microscopy, cultured cells were labeled with an antibody to beta-tubulin followed by a secondary antibody-eosin conjugate. Following confocal imaging of the eosin fluorescence, the specimen is intensely illuminated in the presence of diaminobenzidine. The resulting reactive oxygen creates a reaction product that can be subsequently visualized by electron microscopy (B). (Image kindly provided by the laboratory of Mark Ellisman at the National Center for Microscopy and Imaging Research, University of California, San Diego.)

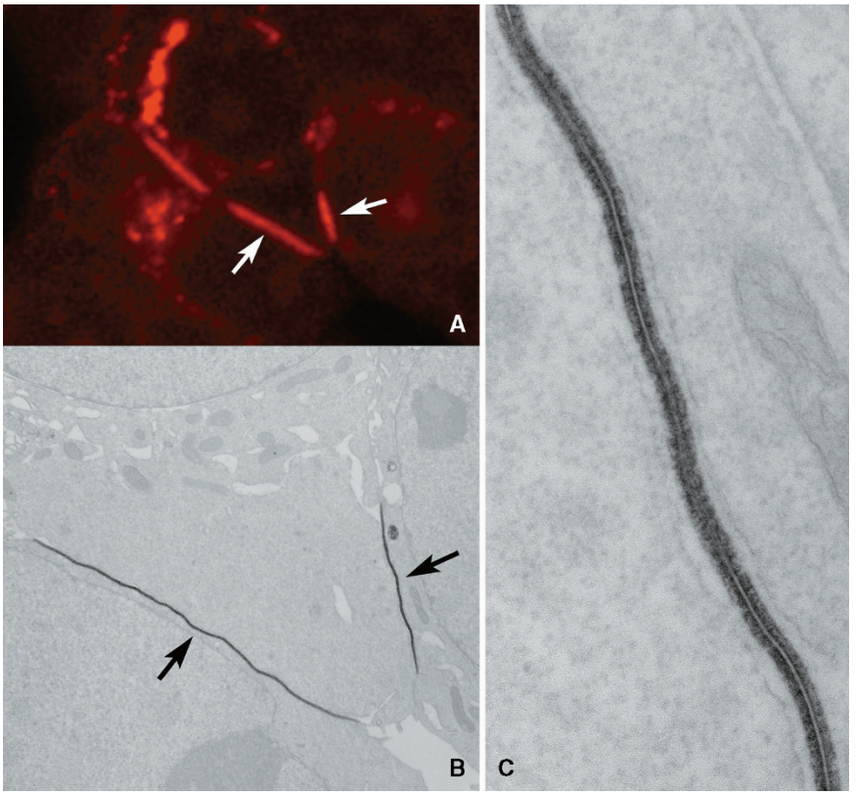

FIGURE 49.15. Using a genetically encoded tetracysteine tag for labeling proteins for light and electron microscopy, cultured cells expressing a recombinant version of the major gap junction protein Cx43 that contains a small tetracysteine tag. Living cells are stained with the biarsenical red fluorescent compound ReAsH (A). Following imaging, the cells are fixed and the specimen is intensely illuminated in the presence of diaminobenzidine. The resulting reactive oxygen creates a reaction product that can be subsequently visualized by electron microscopy (B). (C) is a higher magnification view of (B). (Images kindly provided by the laboratory of Mark Ellisman at the National Center for Microscopy and Imaging Research, University of California, San Diego.)

introduced into the gene of the protein of interest in such a way that the four cysteines can bind to a bi-arsenical derivative of fluorescein (green fluorescence) or resorufin (red fluorescence). Living cells can be bathed in a solution of these membrane-permeant dyes without damage as long as the arsenicals are neutralized with small vicinal dithiols such as 2,3-dimercaptopropanol or 1,2-ethanedithiol. The dye becomes fluorescent only when it bonds specifically to the tetracysteine moiety. Like eosin, the red-fluorescent version of this dye (called ReAsH), is capable of producing reactive oxygen and depositing DAB. The result is a genetically encoded marker that can be seen in both LM (by fluorescence) and TEM (by specific staining) (Gaietta *et al*., 2002; Fig. 49.15). LM/EM correlation can be obtained by embedding the cells still attached to the coverslip and making high- and low-magnification images of them with a confocal microscope before the coverslip is removed. These fluorescent images can them be correlated with low-magnification TEM images of serial-section ribbons made starting from what had been the plastic/coverglass interface.

This same group has also had success labeling structures in such a way that the label can be seen in both LM and EM using quantum dots. These nanocrystals are both fluorescent (Nisman *et al*., 2004) and directly visible in thin-section TEM (Giepmans, 2005; Fig. 49.16). One of the major advantages of using quantum-dot fluorophores is that different colors of quantum dots can be

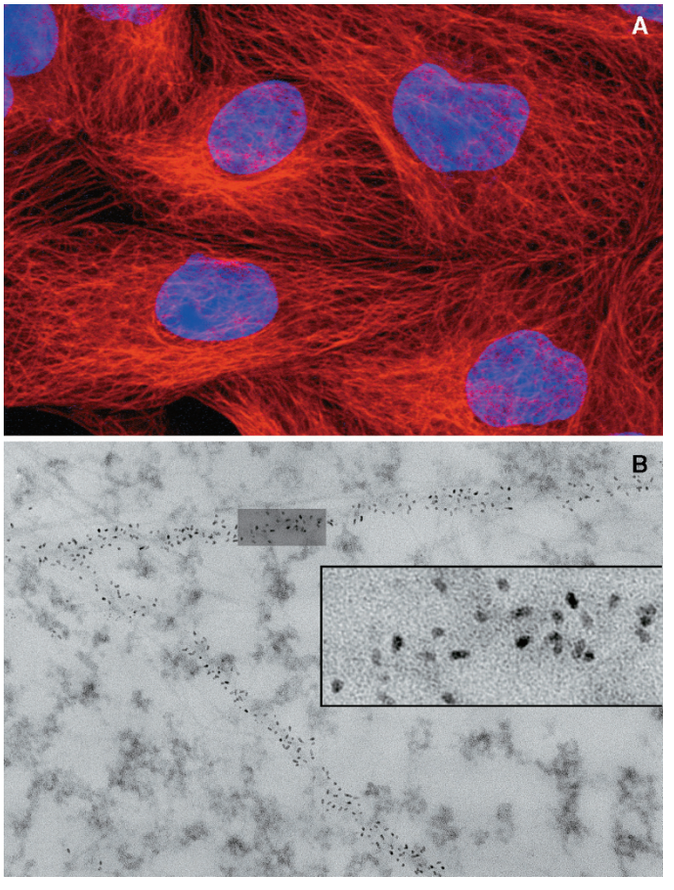

FIGURE 49.16. Using quantum dots as labels for light and electron microscopy, cultured cells were labeled with an antibody to beta-tubulin followed by a secondary antibody-quantum dot 655 conjugate (cell nuclei were counterstained with Hoechst 33342). Following confocal imaging (A), the specimen is prepared for electron microscopy (B). The crystalline core of the quantum dots are readily visible by electron microscopy. (Image kindly provided by the laboratory of Mark Ellisman at the National Center for Microscopy and Imaging Research, University of California, San Diego.)

discriminated by both light and electron microscopy (via size and shape differences), making double or even triple labeling possible. Furthermore, they are not so readily destroyed by electron irradiation as are organic dyes. As a result, it is possible to obtain fluorescent images from the sections after they have been viewed in the TEM. On the other hand, the fluorescence of quantum dots is destroyed if heavy metal stains are used to produce contrast.

Both of these techniques allow one to test and optimize antibody-labeling parameters first by LM before continuing the more laborious processing for electron microscopy.

Marrying Fluorescence with TEM Replicas to Analyze the Cytoskeleton

Phase-contrast and fluorescence microscopy have been used to visualize actin dynamics at the leading edge of living cells in which various cytoskeletal proteins have been labeled with GFP. Svitkina and colleagues followed up such studies by removing the membranes with an extracting buffer, and then shadowing the preparation with Pt after it had been critical-point dried to visualize actin filament structure in the TEM. This led them to propose a filopodial initiation model (Svitkina *et al*., 2003). Such studies provide additional insights into the detailed topology of cytoskeletal assemblies in cells. Because processing for EM is performed on cells with a known history based on LM and potential shrinkage artifacts are carefully monitored during fixation, this approach provides greater confidence that the more highly resolved EM images directly reflect events imaged using LM.

FluoroNanoGold for Cryosections to be Viewed by LM, then TEM

In addition to its utility in analyzing living, migrating cells, viewing specimens first using LM followed by TEM also has other uses. In some cases (e.g., immunostaining), it is far easier to label the structures of interest in fixed and sectioned specimens using LM techniques. Knowing that a given specimen contains the features of interest provides more confidence that subsequent processing for TEM will yield a specimen worth analyzing in detail.

Although it has long been clear that, compared to chemical fixation, cryopreparative techniques both arrest cellular processes faster (milliseconds vs. seconds) and preserve biological structure down to the molecular level better, the complexity of the equipment and procedures needed to freeze even modest-sized specimens without creating ice-crystal artifacts has delayed its widespread use in light microcopy (Biel *et al*., 2003). However, because cryotechniqes are unsurpassed when it comes to preserving antigenicity, in 1998 Takizawa and colleagues stained thin, cryosections with FluoroNanoGold (FNG) antibodies for correlative LM and TEM on the same thin section (Takizawa *et al*., 1998). Ultrathin cryosections were cut from a frozen suspension of fixed cells embedded in gelatin/sucrose. The sections were picked up on finder grids, stained with FNG, and viewed first by fluorescence LM and then by TEM. FluoroNanoGold labels consist of ondeca gold conjugated with a fluorescent dye. As the ondeca gold contains only 11 gold atoms, it often penetrates better than the large colloidal-Au labels. On the other hand, it is difficult to see even in TEM unless it has been decorated by enhancement using silver or gold salts.

Several examples of this technique have been reported. To determine the diameter of transcription sites in the nuclei of HeLa cell, Pombo and colleagues made cryosections 100 to 200 nm thick, stained them with fluorescent antibodies for imaging in the LSCM, and then re-embedded them in Epon to image the same structures by TEM (Pombo *et al*., 1999). In 2001, Robinson reviewed the techniques then used for correlative LM and TEM in cryosections and the advantages of viewing thin sections by LM (Robinson *et al*., 2001).

Any selective staining protocol must face the problem of how to see structure **not** stained with the selective agent. One solution is to use an energy-filtering TEM (EFTEM) to maximize the contrast between unstained protein and embedding resin. Ren and coworkers used this technique to image Quetol-embedded cells in which promyelocytic leukemia (PML)-bodies had been antibody-labeled with Cy-3. They found cyanine and Alexa dyes to be stable in this resin (Ren *et al*., 2003) and also used quantum dots for correlative fluorescence and EFTEM (Nisman *et al*., 2004).

Green Fluorescent Protein Methods

The introduction of the genetically based marker, green fluorescent protein (GFP), has revolutionized the study of cell biology (see Chapter 16, *this volume*). In 2003, Luby-Phelps showed that GFP fluorescence, which was destroyed by most TEM embedding techniques, survived embedding in LR White (Luby-Phelps *et al*., 2003). Adjacent thin and 1 μm sections were cut from preparations of zebrafish eyes and viewed using the TEM and LM, respectively.

Recently, we have extended this approach to thin sections. Specifically, we were interested in the relationship between two junction proteins, HMP-1 [*Caenorhabditis elegans (Ce)* alpha-catenin] and DLG-1 (*Cediscs* large). Confocal fluorescence LM had shown that DLG localizes near HMP-1. To find out if these molecules colocalized at the EM level, we imaged HMP-1::GFP in a thin section by LSCM and immuno-gold-labeled DLG-1 in the same section. EM localization of DLG-1 gold particles with HMP-1::GFP expression is consistent with LM data and confirms the gold labeling parameters needed to label DLG. Thin sections, adhered to EM finder grids and floating on coverslips, were first imaged in an LSCM using both fluorescence and backscattered light (BSL), to reveal the section surface [Fig. 49.17(A)], and fluorescence, to show HMP-1::GFP [Fig. 49.17(B)]. The combination of BSL (displayed in red) and GFP, in green [Fig. 49.17(C)], shows the location of GFP within each embryo and is useful for locating a specific embryo in the TEM [Fig. 49.17(D)]. At higher magnification, the boxed area shows the 20 nm gold labeling due to DLG-1 [Fig. 49.17(F)].

We have also imaged AJM-1::GFP (a novel *Ce* junction molecule) in the pharynx with 20 nm-gold anti-GFP in LR-Gold thin sections after chemical fixation [Fig. 49.18(A)]. Although colloidal gold particles have been shown to quench the fluorescence of molecules in close proximity to them (Kandela *et al.*, 2004), we have found that rhodamine-linked secondary antibodies, not actually conjugated to the gold-label [Fig. 49.18(B)] still fluoresce [Fig. 49.18(C)] (Sims and Hardin, 2004). Like the ReAsH system mentioned above, this procedure also allows one to visualize a genetic marker in a thin section, using both fluorescence LM and a specific stain visible in TEM.

Using Phalloidin as a Correlative Marker

As GFP fluorescence had been shown to survive dehydration and embedding in methacrylate resin, we were curious if rhodamine–phalloidin might also survive this process. *C. elegans* embryos that had been bleached to remove the eggshell, were fixed and incubated in buffer containing saponin and rhodamine–phalloidin. After low-temperature embedding in LR-Gold, 100 nm sections were cut and imaged by confocal laser scanning

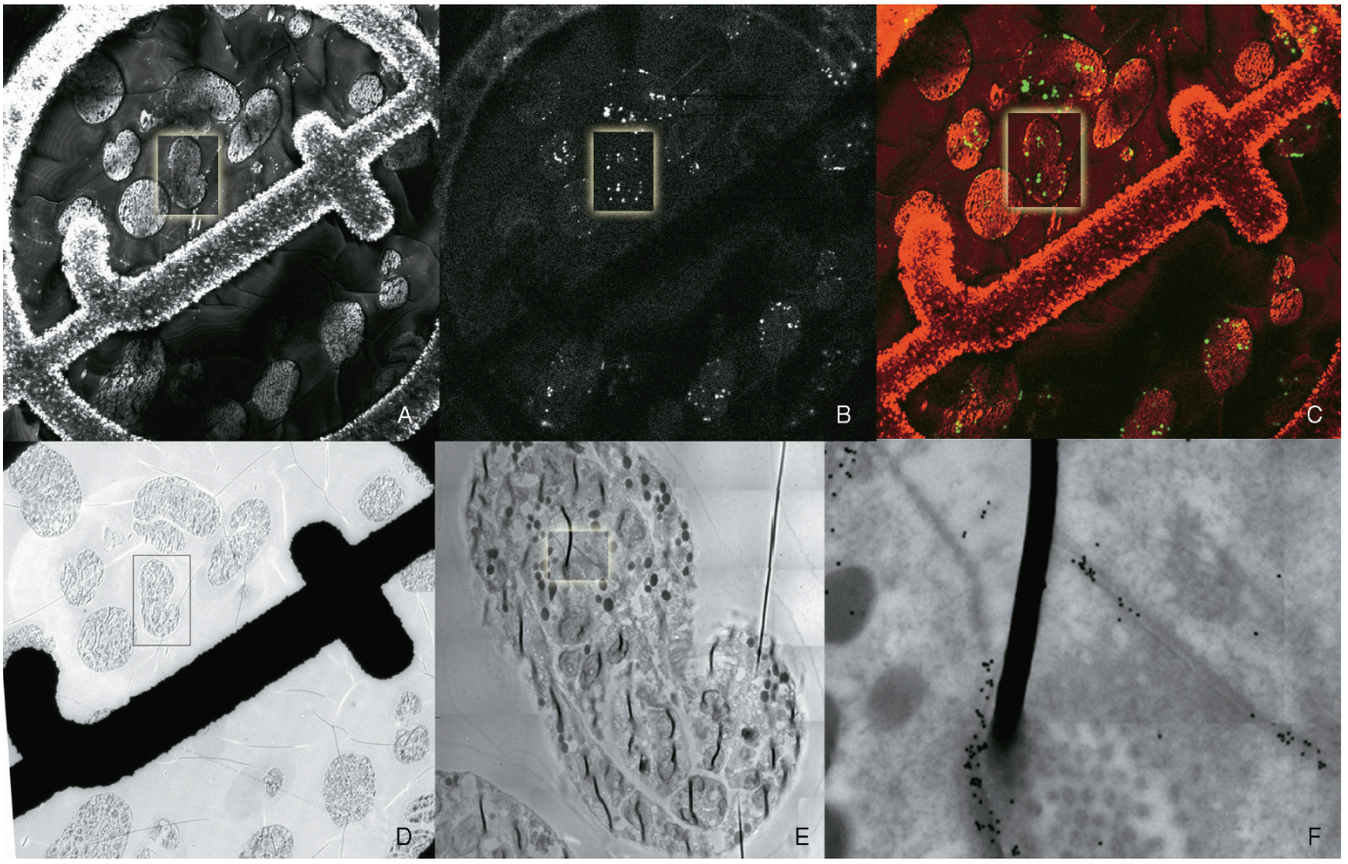

FIGURE 49.17. (A) BSL image of a thin section on an EM finder grid. (B) HMP-1::GFP from the same thin section. (C) A red-green merge of BSL and GFP images which is useful to orient fluorescence to specific embryos. (D) TEM of the same area imaged in (A–C) with the same embryo highlighted by the boxed area. (E) Higher magnification TEM montage of the comma-staged embryo also observed in all previous figures. (F) Boxed area in (E) with 20 nm gold labeling DLG-1, a junctional protein that colocalizes with AJM-1.

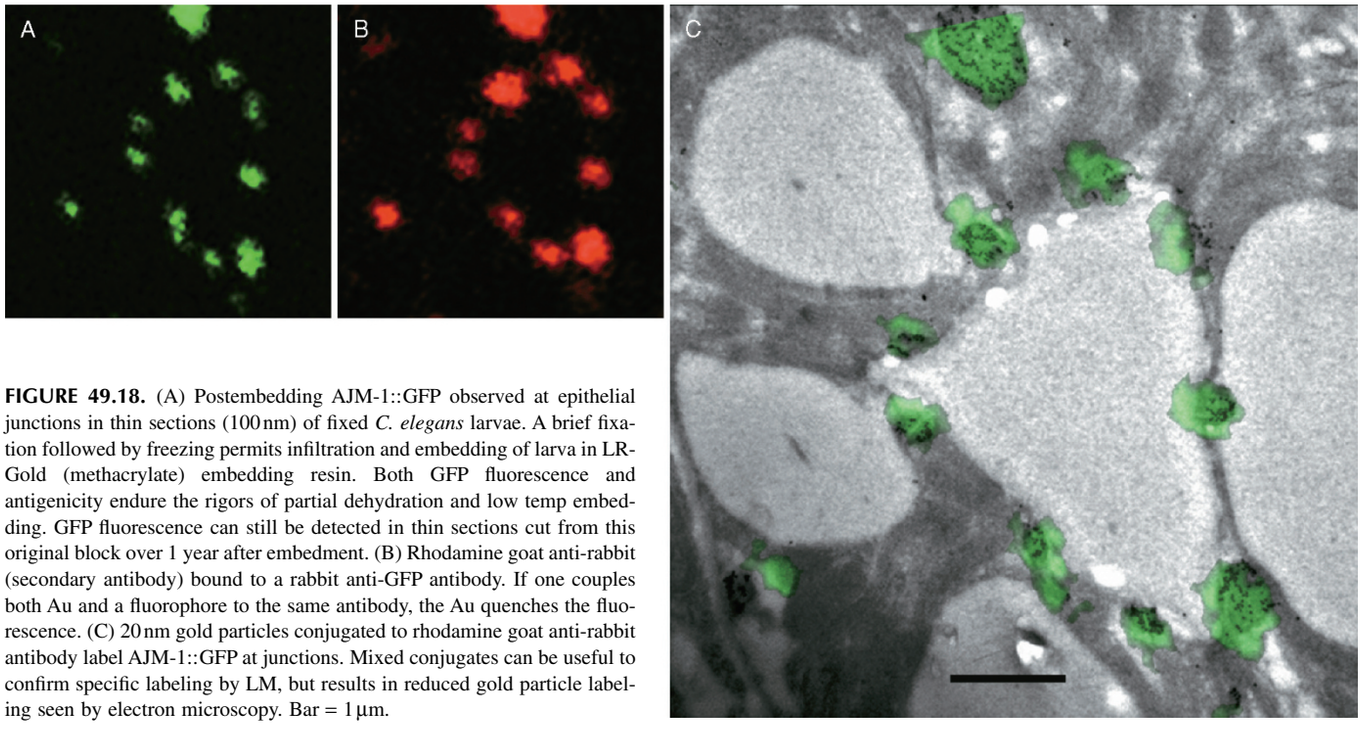

FIGURE 49.18. (A) Postembedding AJM-1::GFP observed at epithelial junctions in thin sections (100 nm) of fixed *C. elegans* larvae. A brief fixation followed by freezing permits infiltration and embedding of larva in LR-Gold (methacrylate) embedding resin. Both GFP fluorescence and antigenicity endure the rigors of partial dehydration and low temp embedding. GFP fluorescence can still be detected in thin sections cut from this original block over 1 year after embedment. (B) Rhodamine goat anti-rabbit (secondary antibody) bound to a rabbit anti-GFP antibody. If one couples both Au and a fluorophore to the same antibody, the Au quenches the fluorescence. (C) 20 nm gold particles conjugated to rhodamine goat anti-rabbit antibody label AJM-1::GFP at junctions. Mixed conjugates can be useful to confirm specific labeling by LM, but results in reduced gold particle labeling seen by electron microscopy. Bar = 1 μm.

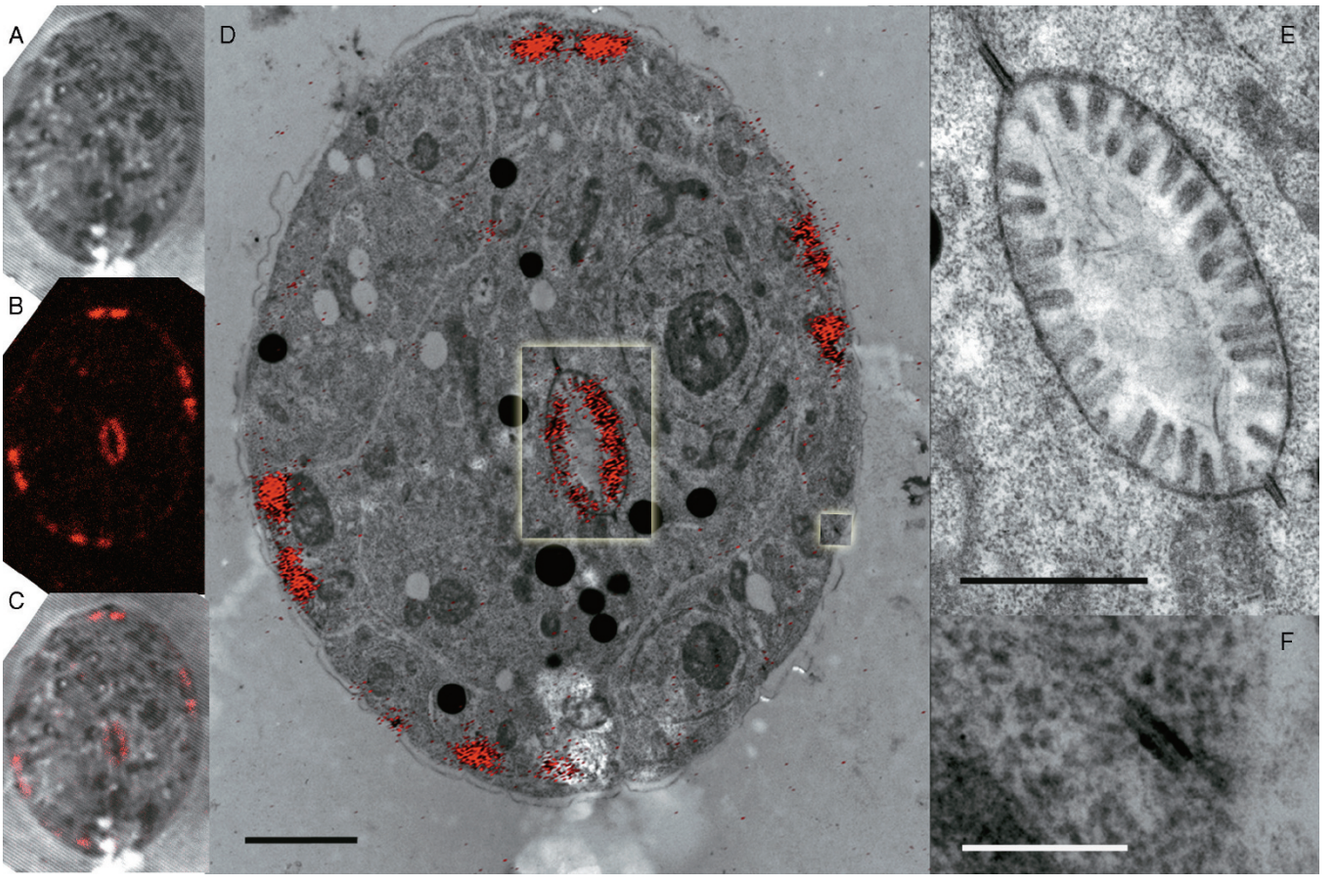

FIGURE 49.19. TEM cross-section of a *C. elegans* larva, *en bloc*-stained with rhodamine-phalloidin and viewed simultaneously in backscattered (A) and fluorescent (B) light on a confocal microscope. (C) Overlay of (A) and (B). (D) A low-magnification TEM (bar = 2 µm). The two boxed areas are seen at higher magnification in (E), a close-up of the intestine (bar = 1 µm) and (F) a hypodermal adherens junction (bar = 0.5 µm). Phalloidin staining is seen decorating the intestinal microvilli and the four muscle quadrants on the sides of the worm.

microscopy (CLSM). A BSL image [Fig. 49.19(A)] and a fluorescent image [Fig. 49.19(B)] were merged together [Fig. 49.19(C)] showing actin-rich, phalloidin-stained muscle quadrants and intestinal microvilli in red. The contrast from the rhodamine signal was increased and overlayed on a low-magnification TEM image [Fig. 49.19(D)]. The boxed regions in Figure 49.19(D) are shown at higher magnification in Figure 49.19(E), covering the intestinal microvilli, and Figure 49.19(F), showing an adherens junction. Overall, this study demonstrates that, at least for proteins as concentrated as actin in muscle and microvilli, one can assess which structures are labeled by analyzing only the fluorescent LM images.

Cryo-Immobilization Followed by Post-Embedding Confocal Laser Scanning Microscopy on Thin Sections

Chemical fixation is known to be slow and to introduce a wide variety of artifacts. Unfortunately, the only alternative is cryopreservation, a technique that depends for its success on freezing the important part of the specimen without forming detectable ice-crystal artifacts. At atmospheric pressure, ice crystals can only be avoided by using cryoprotectants, such as sucrose and polyethylene glycol, or by freezing the tissue very fast indeed (>10^5 K/s; Studer *et al*., 1989; McDonald *et al*., 1993). As using a cryoprotectant requires at least some prefixation, it is not a great improvement on other types of chemical fixation. However, fast freezing is also complex; largely because of the high heat-of-fusion of water and the low thermal conductivity of ice, even cryogens as efficient as liquid-He–cooled copper are unable to extract the heat from the specimen fast enough to prevent ice-crystal artifacts from more than the outer 10 to 15 µm of the specimen.

Objects the size of *C. elegans* (60 µm diameter) can only be successfully frozen using a high-pressure freezer (Studer *et al*. 1989; McDonald *et al*., 1993). In this device, pressurized LN_2 is used to cool a specimen about 2 mm in diameter and 200 µm thick from ambient temperature to 77 K in about 20 ms, under a transient pressure spike of about 2000 bar. Under these conditions, water freezes at a lower temperature (~253 K rather than 273 K), and ice crystals propagate more slowly for various reasons, including the fact that the viscosity of the water increases with ambient pressure. The result is that a relatively high fraction of such specimens are frozen without noticeable artifact.

For TEM observation, freezing is followed by either freeze fracture/metal shadowing/carbon replication, or freeze substitution with ethanol or acetone followed by "normal" epoxy embedment in Lowicryl HM-20. With the latter approach, the plastic-

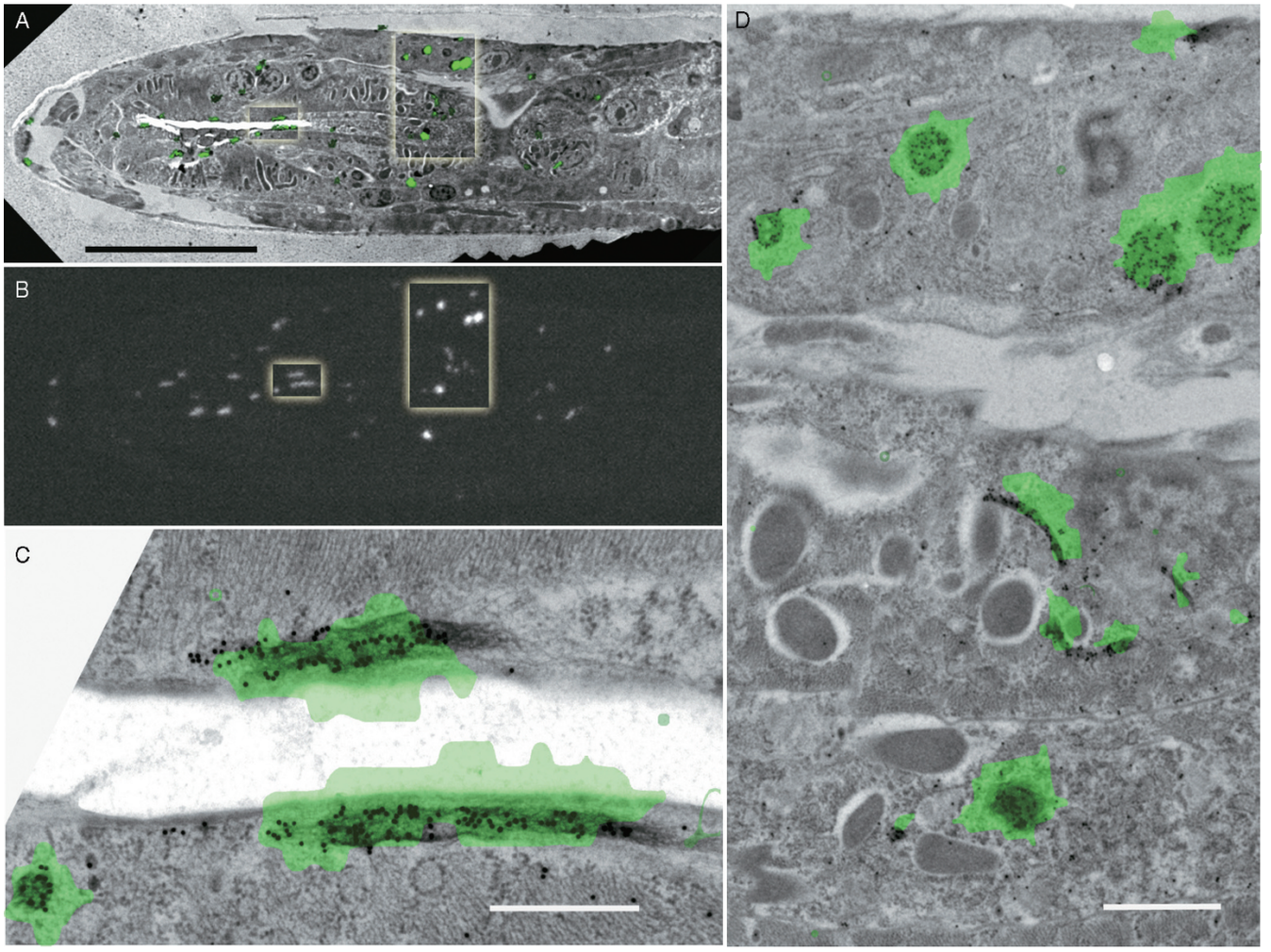

FIGURE 49.20. (A) TEM longitudinal section of an adult *C. elegans*. (B) The same section viewed by fluorescent confocal microscopy showing that the fluorescence of AJM-1::GFP has not been eliminated by embedding in LR-Gold. Boxed areas in (A) and (B) are shown at higher magnification in (C) and (D), where the fluorescence image has been overlaid in green over the TEM image. As the section was also labeled with anti-GFP-gold, these insets show good agreement between the distribution of these two markers in pharynx (C) and around the gut (D). Bar = (A, B) 10 µm; (C) 0.5 µm; (D) 1 µm.

embedded specimen can be viewed directly using CLSM, and this image can be used to choose the best area of the block to be sectioned for TEM (Biel *et al*., 2003).

Cryopreparation of *C. elegans*

Because the eggshell and the vitelline membrane reduce penetration by chemical fixatives, *C. elegans* embryos are difficult to fix chemically. As a result, we have adapted the freeze-substitution protocol to prevent it from damaging frozen GFP specimens. Although Ward observed that GFP fluorescence was completely extinguished if specimens were placed in absolute ethanol (Ward, 1998), Walther and Ziegler (2002) found that adding 1% to 5% water to the freeze-substitution medium increased the visibility of membranes, and we reasoned that a similar approach might preserve GFP structure. We found that freeze substitution in 95% ethanol/5% water, followed by low-temperature embedding in LR Gold, preserves AJM-1::GFP in thin sections (Fig. 49.20). Figure 49.20(B) shows a thin section of a specimen containing AJM-1::GFP and also stained with Au-conjugated anti-GFP, imaged with a disk-scanning confocal microscope. In Figure 49.20(A), an image of GFP fluorescence is overlaid on a low-magnification TEM image. Higher magnification TEMs of the two areas highlighted in Figure 49.20(B) are shown in Figure 49.20(C,D). The green overlays roughly colocalize with the 20 nm gold label.

This technique allows one to combine the ability of fluorescence LM to search large areas of the section rapidly to identify rare stained structures and then find and view these rare structures in the TEM. The result confirms that this HPF protocol preserves GFP fluorescence and specimen immunoreactivity and also allows one to correlate AJM-1::GFP with specific cellular structures visible only at the ultrastructural level.

Another application of GFP and cryopreservation involves identification of wild-type and mutant embryos prior to cryopreservation and processing with immunogold. Although *C. elegans* embryos containing mutant copies of the *ajm*-1 gene arrest soon after the 2-fold stage, an average 60% of them can be rescued to viability if the hermaphrodite (parent) is microinjected with an extrachromosomal array that includes a functional copy of the

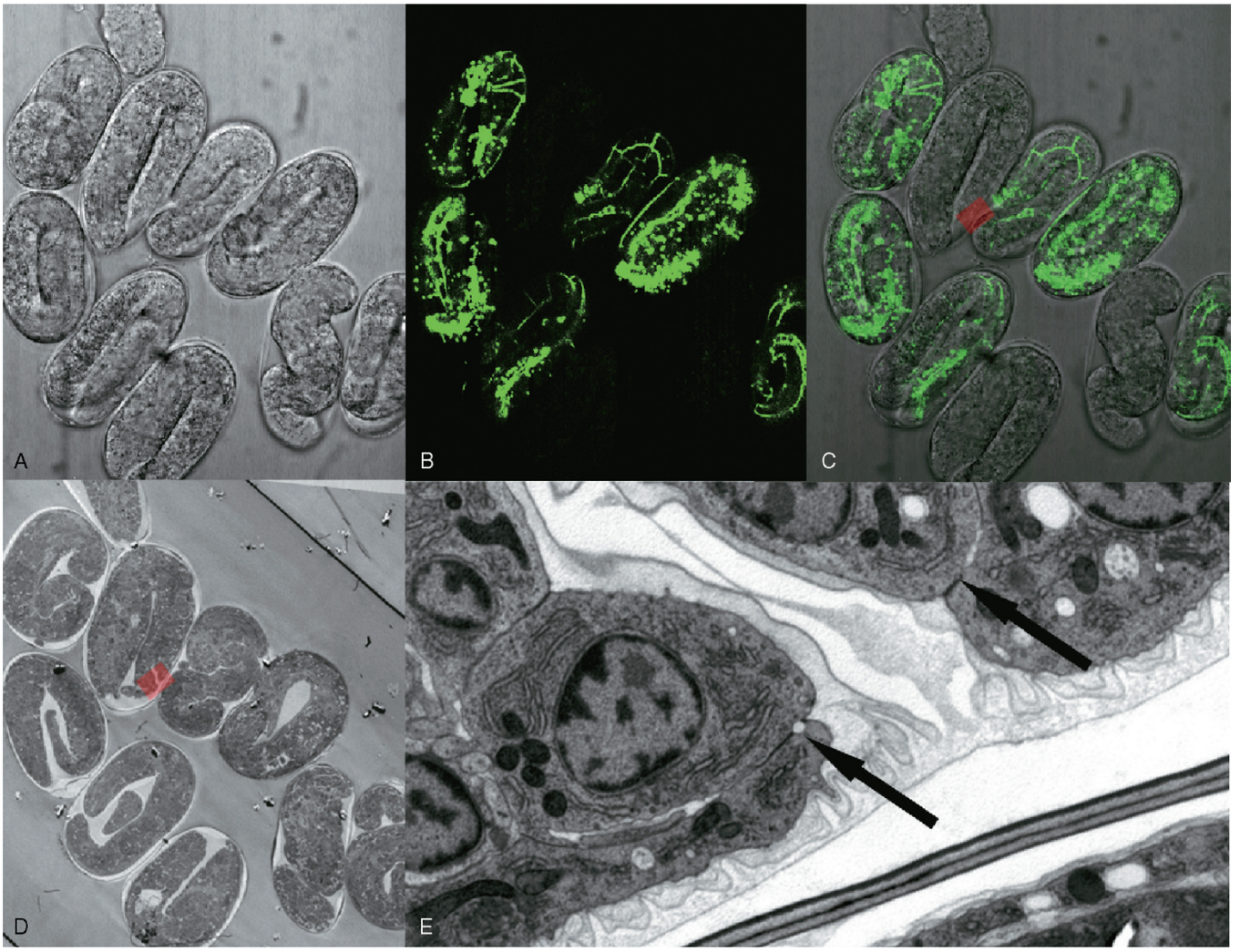

FIGURE 49.21. (A) A transmitted light image of living embryos embedded in agar. (B) A brightest-pixel projection (ImageJ) of AJM-1::GFP expression in the same embryos in (A). Transmitted light and fluorescence images were obtained simultaneously on a Bio-Rad 1024 confocal using 488 nm excitation. Embryos older than comma stage which do not express GFP, lack the *ajm*-1 gene. (C) Overlay of the fluorescent projection over the transmitted light image. Red-shaded area is a 2-fold embryo which lacks *ajm*-1. (D) A TEM image of the same embryos after HPF and embedding in Epon. Same area red-highlighted in (C) and (D) is shown in (E), where arrows point to epithelial cell membrane separations associated with the loss of *ajm*-1.

ajm-1 gene, in this case *ajm*-1 fused to the GFP-coding region. The GFP label allows the observer to determine which of the living embryos carry the *ajm*-1 gene and which do not. Although one could make a similar discrimination by applying Au-conjugated, anti-GFP antibodies to the thin sections, optimal fixation and staining could be compromised by the need to preserve the antigenicity of the GFP. Correlating the LM fluorescence image of a living embryo with the TEM image of a section from this embryo avoids this problem, particularly if rescued and non-rescued embyos are next to one another on the same TEM grid. Any observable differences are more likely to be real when one knows that the high-pressure freezing, fixation, and staining are identical.

Figure 49.21(A) shows a transmitted light image of a group of 10 embryos, 6 of which have been rescued (Koppen *et al*., 2001; Simske *et al*., 2003). Although the non-rescued embryos look normal in transmitted light, they are clearly marked by the absence of GFP fluorescence [Fig. 49.21(B,C)]. Following high-pressure freezing, freeze substitution, embedding in Epon, and sectioning, the same group of embryos can be visualized at low magnification by TEM [Fig. 49.21(D)]. The small red-shaded boxes in Figure 49.21(C,D) indicate the area shown at higher magnification in Figure 49.21(E). Arrows point to separations at epithelial cell junctions believed to be associated with the loss of *ajm*-1.

Tiled Montage Transmission Electron Microscope Images Aid Correlation

Many modern TEMs incorporate both electronic image recording and motor-driven stage motion. This combination of features greatly facilitates LM/TEM correlational studies by making it much easier to obtain high-resolution images over a wide area of the specimen. Figure 49.22 shows such a tiled montage of a specimen prepared in the same way as that shown in Figure 49.21. This image covers an area $30 \times 50\,\mu m$ in size and consists of 36 images recorded at an original magnification of 3.5×. The green overlay represents AJM-1::GFP fluorescence recorded on a Bio-Rad 1024 confocal microscope.

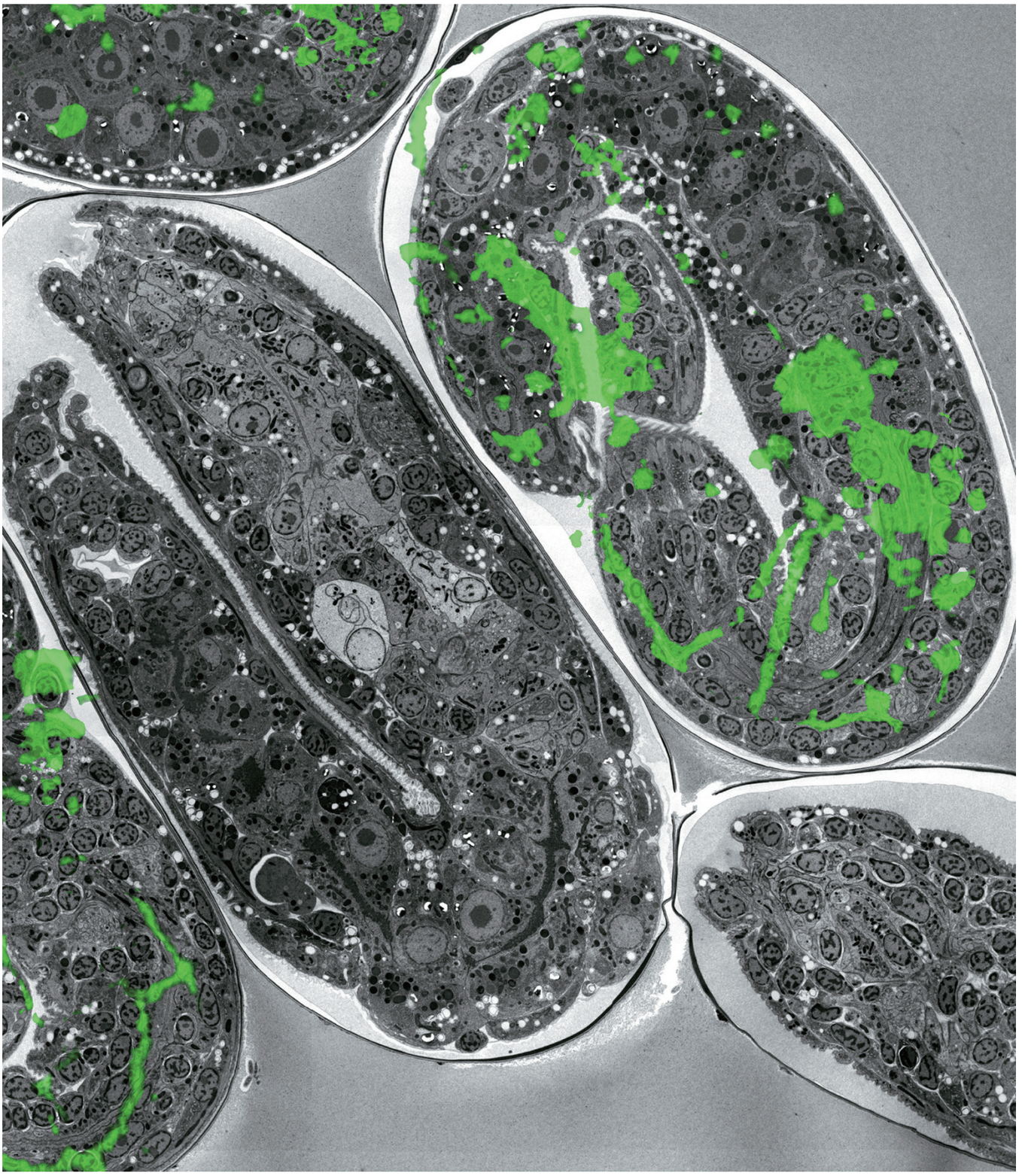

FIGURE 49.22. A tiled montage TEM image of a specimen prepared in the same way as that shown in Figure 49.11. The original montage covered an area of the specimen 50 × 32 µm in size and consisted of 36 images recorded at 80 kV using an original magnification of 3400× on a Phillips 120 using a Soft Imaging Systems, Keenview, CCD camera coupled to the phosphor by a 3.4× fiber-optic taper. The green overlay represents AJM-1::GFP fluorescence recorded on a Bio-Rad 1024 confocal microscope.

CONCLUSION

Although during the 1950s and 1960s light microscopy languished beneath the high-resolution shadow of the electron microscope, starting in the early 1970s, it flowered as a variety of new technical improvements were introduced: video-enhanced DIC, video-intensified fluorescence, improved CCD cameras, and myriad new fluorescent probes. Suddenly, the fact that one could observe function in wholly new ways seemed to more than offset the ability to image the internal features of intracellular organelles. These LM developments were soon followed in the 1980s and 1990s by the widespread use of a variety of confocal microscopes, and more recently by the advent of GFP and its many relations. This entire book is a testament to the fact that live-cell fluorescent light microscopy is blossoming as never before.

On the other hand, we lose nothing by admitting that much of the business of cells occurs at a size scale that is much smaller than that which can be imaged with the light microscope. When this occurs, it is useful to remember that help is at hand; given the effort needed to boost LM spatial resolution by a factor of 2, it is salutary to acknowledge how much more clearly one can see when it is increased by a factor of 40.

ACKNOWLEDGMENTS

This work was supported by grants from the National Institutes of Health: GM-058038 (Hardin), RR-04050 (Ellisman), and NIGMS-63001 (Albrecht); and from the National Science Foundation IBN-0712803 (Hardin).

REFERENCES

Albrecht, R.M., Goodman, S.L., and Simmons, S.R., 1989, Distribution and movement of membrane-associated platelet glycoproteins: Use of colloidal gold with correlative video-enhanced light microscopy, low-voltage high-resolution scanning electron microscopy, and high-voltage transmission electron microscopy, *Am. J. Anat.* 185:149–164.

Albrecht, R.M., Olorundare, O.E., Simmons, S.R., Loftus, J.C., and Mosher, D.F., 1992, Use of correlative microscopy with colloidal gold labeling to demonstrate platelet receptor distribution and movement, *Methods Enzymol.* 215:456–479.

Biel, S.S., Kawaschinski, K., Wittern, K.P., Hintze, U., and Wepf, R., 2003, From tissue to cellular ultrastructure: Closing the gap between micro- and nanostructural imaging, *J. Microsc.* 212:91–99.

Deerinck, T.J., Martone, M.E., Lev-Ram, V., Green, D.P., Tsien, R.Y., Spector, D.L., Huang, S., and Ellisman, M.H., 1994, Fluorescence photooxidation with eosin: A method for high resolution immunolocalization and *in situ* hybridization detection for light and electron microscopy, *J. Cell Biol.* 126:901–910.

Gaietta, G., Deerinck, T.J., Adams, S.R., Bouwer, J., Tour, O., Laird, D.W., Sosinsky, G.E., Tsien, R.Y., and Ellisman, M.H., 2002, Multicolor and electron microscopic imaging of connexin trafficking, *Science* 296: 503–507.

Giepmans, B.N., Deerinck, T.J., Smarr, B.L., Jones, Y.Z., and Ellisman, M.H., 2005, Correlated light and electron microscopic imaging of multiple endogenous proteins using Quantum dots, *Nature Methods* 2(10):743–749.

Gorbsky G.J., Sammak, P.J., and Borisy, G.G., 1987, Chromosomes move poleward in anaphase along stationary microtubules that coordinately disassemble from their kinetochore ends, J. *Cell Biol*. 104:9–18.

Griffin, B.A., Adams, S.R., and Tsien, R.Y., 1998, Specific covalent labeling of recombinant protein molecules inside live cells, *Science* 281:269–272.

Kandela, I.K., Bleher, R., and Albrecht, R.M., 2004, Correlative labeling studies in light and electron microscopy, *Microsc. Microanal*. 10(Suppl, 2):1212–1213.

Koppen, M., Simske, J.S., Sims, P.A., Firestein, B.L., Hall, D.H., Radice, A.D., Rongo, C., and Hardin, JD., 2001, Cooperative regulation of AJM-1 controls junctional integrity in *Caenorhabditis elegans* epithelia, *Nat. Cell Biol.* 3:983–991.

Loftus, J.C., Choate, J., and Albrecht, R.M., 1984, Platelet activation and cytoskeletal reorganization: High voltage electron microscopic examination of intact and Triton-extracted whole mounts, *J. Cell Biol.* 98:2019–2025.

Luby-Phelps, K., Ning, G., Fogerty, J., and Besharse, J.C., 2003, Visualization of identified GFP-expressing cells by light and electron microscopy, *J. Histochem. Cytochem.* 51:271–274.

Maranto, A.R., 1982, Neuronal mapping: A photooxidation reaction makes Lucifer yellow useful for electron microscopy, *Science* 217:953–955.

McDonald, K., and Morphew, M.K., 1993, Improved preservation of ultrastructure in difficult-to-fix organisms by high-pressure freezing and freeze-substitution: I. *Drosophila melanogaster* and *Strongylocentrotus purpuratus* embryos, *Microsc. Res. Tech*. 24:465–473.

Nisman, R., Dellaire, G., Ren, Y., Li, R., and Bazett-Jones, D.P., 2004, Application of quantum dots as probes for correlative fluorescence, conventional, and energy-filtered transmission electron microscopy, *J. Histochem. Cytochem.* 52:13–18.

Pawley, J.B., 1990, Practical aspects of high resolution LVSEM, *Scanning* 12:247–252.

Pawley, J.B., 1992, LVSEM for high resolution topographic and density contrast imaging, *Adv. Electron. Electron Phys*. 83:203–274.

Pawley, J.B., and Albrecht, R., 1988, Imaging colloidal gold labels in LVSEM, *Scanning* 10:184–189.

Pawley, J.B., Sepsenwol, S., and Ris, H., 1986, Four-dimensional microscopy of *Ascaris* sperm motility, *Ann. N Y Acad. Sci.* 483:171–180.

Pombo, A., Hollinshead, M., and Cook, P.R., 1999, Bridging the resolution gap: Imaging the same transcription factories in cryosections by light and electron microscopy, *J. Histochem. Cytochem.* 47:471–480.

Ren, Y., Kruhlak, M.J., and Bazett-Jones, D.P., 2003, Same serial section correlative light and energy-filtered transmission electron microscopy, *J. Histochem. Cytochem.* 51:605–612.

Robinson, J.M., Takizawa, T., Pombo, A., and Cook, P.R., 2001, Correlative fluorescence and electron microscopy on ultrathin cryosections: Bridging the resolution gap, *J. Histochem. Cytochem.* 49:803–808.

Sepsenwol, S., Ris, H., and Roberts, T.M., 1989, A unique cytoskeleton associated with crawling in the amoeboid sperm of the nematode, *Ascaris suum*, *J. Cell Biol.* 108:55–66.

Sepsenwol, S., and Taft, S.J., 1990, *In vitro* induction of crawling in the amoeboid sperm of the nematode parasite, *Ascaris suum*, *Cell Motil. Cytoskeleton* 15:99–110.

Sims, P.A., and Hardin, J.D., 2004, Visualizing green fluorescent protein and fluorescence associated with a gold conjugate in thin sections with correlative confocal and electron microscopy, *Microsc. Microanal*. 10(Suppl. 2):156–157.

Simske, J.S., Koppen, M., Sims, P., Hodgkin, J., Yonkof, A., and Hardin, J., 2003, The cell junction protein VAB-9 regulates adhesion and epidermal morphology in *C. elegans* [comment], *Nat. Cell Biol.* 5:619–625.

Studer, D., Michel, M., and Muller, M., 1989, High-pressure freezing comes of age, *Scanning* 11(Suppl. 3):253–269.

Svitkina, T.M., Bulanova, E.A., Chaga, O.Y., Vignjevic, D.M., Kojima, S., Vasiliev, J.M., and Borisy, G.G., 2003, Mechanism of filopodia initiation by reorganization of a dendritic network, *J. Cell Biol*. 160:409–421.

Takizawa, T., Arai, S., Osumi, M., and Saito, T., 1998, Ultrastructure of human scalp hair shafts as revealed by freeze-substitution fixation, *Anat. Rec.* 251:406–413.

Walther, P., and Ziegler, A., 2002, Freeze substitution of high-pressure frozen samples: The visibility of biological membranes is improved when the substitution medium contains water, *J. Microsc*. 208:3–10.

Ward, W.W., 1998, *Green Fluorescent Proteins: Proteins, Applications and Protocols*, John Wiley and Sons, New York.

Wetzel, B., Erickson, B.W., and Levis, W.R., 1973, The need for positive identification of leukocytes examined by SEM, Part III:535–541.